A study of ozone variability and its connection with meridional transport in the northern Pacific lower stratosphere during summer 2002

Thierry Leblanc and I. Stuart McDermid
Table Mountain Facility, Jet Propulsion Laboratory, California Institute of Technology, Wrightwood, California, USA

Alain Hauchecorne
Service d'Aeronomie du CNRS, Verrieres-le-Buisson, France

Received 30 July 2003; revised 23 February 2004; accepted 9 March 2004; published 4 June 2004.

[1] A preliminary study of the impact of the north-central Pacific circulation in the subtropical stratosphere on ozone variability locally observed by lidar is presented. The results from the upper tropospheric and stratospheric ozone measurements of the Jet Propulsion Laboratory lidars located at Mauna Loa Observatory (MLO), Hawaii, and Table Mountain Facility (TMF), California, during summer 2002 were compared to isentropic potential vorticity (IPV) advected on 54 levels from 320 to 1500 K by the high-resolution model MIMOSA. The correlation between ozone measured by lidar, and the origin of the 10-day backward trajectories of the air parcels sampled, was also investigated. Near the tropopause, strong positive correlation between ozone mixing ratio and IPV was observed at both MLO and TMF lidar sites. The largest fluctuations were centered near 350 K and are associated with the meridional displacement of the tropopause by Rossby waves north or south of the observing sites. These large displacements were occasionally accompanied by Rossby wave breaking (RWB), as was identified several times during the summer in the vicinity of the Hawaiian Islands. Using IPV maps, a case study of the 13 July event is briefly presented. This event appears to be typical of breaking events previously investigated at midlatitudes, including the southward intrusion of high-PV air originating in the high-latitude lower stratosphere. This time the intrusion was observed to extend deep in the subtropics. Strong positive ozone anomalies were simultaneously measured by the MLO lidar. Positive correlation between ozone and the equivalent latitude averaged along the parcels' trajectories was seen up to 475 K in the stratosphere. At and above 750 K, negative correlation was calculated for both TMF and MLO. For TMF the altitude dependence of the correlation is similar to that already observed for summer and winter midlatitudes For MLO the observed negative correlation was found to be the result of opposite seasonal and interannual tendencies in ozone and equivalent latitude throughout the summer. All other correlations are associated with a higher intraseasonal variability of both ozone and the parcels' origin, as compared to their seasonal tendencies. *INDEX TERMS:* 0341 Atmospheric Composition and Structure: Middle atmosphere—constituent transport and chemistry (3334); 0368 Atmospheric Composition and Structure: Troposphere—constituent transport and chemistry; 3334 Meteorology and Atmospheric Dynamics: Middle atmosphere dynamics (0341, 0342); 3360 Meteorology and Atmospheric Dynamics: Remote sensing; 3362 Meteorology and Atmospheric Dynamics: Stratosphere/troposphere interactions; *KEYWORDS:* ozone transport, lower stratosphere, tropopause

Citation: Leblanc, T., I. S. McDermid, and A. Hauchecorne (2004), A study of ozone variability and its connection with meridional transport in the northern Pacific lower stratosphere during summer 2002, *J. Geophys. Res.*, *109*, D11105, doi:10.1029/2003JD004027.

1. Introduction

[2] Research on stratosphere-troposphere exchange (STE) and meridional transport in the stratosphere is needed to understand processes that affect long-term changes of tropospheric and stratospheric constituents, such as ozone or water vapor, and subsequently to understand their role in climate change both above and below the tropopause. An average ozone decline of 0.8% per decade in the upper stratosphere and 0.3% per decade in the lower stratosphere was found at midlatitudes during the 1980s and early 1990s using data from different instruments [*Reinsel et al.*, 1999;

Copyright 2004 by the American Geophysical Union.
0148-0227/04/2003JD004027$09.00

Newchurch et al., 2000]. A decline that could neither be explained by simply the observed cooling of the stratosphere, nor by large-scale springtime dilution of ozone-depleted polar air masses. More recently, *Remsberg et al.* [2001] showed that satellite data indicated this decline did not continue through the mid and late 1990s. After separating the origin of the air parcels sampled during 32 winters above Arosa, Switzerland, *Koch et al.* [2002] suggested that the midlatitude ozone partial pressure decline in the upper stratosphere could be a consequence of polar ozone depletion, while the decline observed in the lower stratosphere could result from an increased transport of ozone-poor air from the subtropics. However, using the example of the November 2000 ozone minihole event over Europe, *Semane et al.* [2002] showed that the very low ozone episodes sometimes observed over Europe can also be explained by the uplift of isentropic surfaces in the lowermost stratosphere during such events, instead of isentropic transport of ozone-poor air masses from the subtropics. One crucial aspect of atmospheric transport is how much of a constituent like ozone is transported across barriers such as the tropopause, or so-called stratospheric "subtropical transport barriers" [e.g., *Chen et al.*, 1994; *Grant*, 1989; *Waugh*, 1996]. In this respect, measuring and understanding the lower stratospheric ozone variations in the subtropics on many timescales, ranging from intraseasonal to interannual, and connecting the observed variations to possible variations in transport, emerges as a major research topic. In the framework of the international Network for the Detection of Stratospheric Change (NDSC), the Jet Propulsion Laboratory (JPL) has developed three ozone lidar systems for long-term tropospheric and stratospheric measurements at the Table Mountain Facility (TMF), California (34.4°N), and Mauna Loa Observatory (MLO), Hawaii (19.5°N). The 15 years of stratospheric ozone measurements at TMF, and 10 years at MLO thus constitute valuable sources of information typical of the subtropics.

[3] Interestingly, both the MLO and TMF locations have been identified as strongly active STE regions due to the particular configuration of the circulation in the upper troposphere-lower stratosphere (UTLS) over the Pacific Ocean, specifically at the "exit" of the Asian monsoon upper circulation. Using maps of isentropic Ertel's potential vorticity (referred to as IPV throughout this paper), *Hoskins* [1991] pointed out that significant meridional, and subsequently stratosphere-to-troposphere (STT) (respectively troposphere-to-stratosphere (TST)) transport occurs at 360 K in the eastern (respectively western) side of the subtropical anticyclone associated with the Asian summer monsoon (located over the Tibetan Plateau and China). Many STE studies have since emphasized the importance of the Asian summer monsoon. *Chen* [1995] showed that STT occurs in all seasons below 330 K but exhibits a clear annual cycle at and above 340 K with a maximum in summer east of the Asian Monsoon Highs (subtropical northwestern Pacific). TST exhibits a similar maximum west of it. Additionally, *Dunkerton* [1995] showed that equatorward motions occur preferentially at the exit of the jet stream while poleward motions occur preferably at the entrance. Based on Dunkerton's results, *Chen* [1995] suggested the presence of a subtropical surf zone, similar to that described by *McIntyre and Palmer* [1984] at the edge of the stratospheric polar winter vortex, but where Rossby wave breaking (RWB) occurs preferentially at critical surfaces near the subtropical tropopause. These RWB events are represented on isentropic maps of PV by the irreversible deformation of the PV contours due to the reversal of the meridional PV gradient toward large (unstable) negative values. In the Northern Hemisphere, these deformations produce large positive (respectively negative) PV anomalies during what is now called "equatorward" (respectively "poleward") breaking events. RWB events therefore appear to be a significant source of mixing in the subtropics and should be fully understood and quantified.

[4] Above the UTLS region (approximately 415 K and higher), a high degree of correlation between PV and ozone exists in the winter midlatitude surf zone and has been widely reported [e.g., *Koch et al.*, 2002]. Well-mixed air masses of various ages tend to reduce this correlation in the summer midlatitudes [*Calisesi et al.*, 2001]. In contrast to the well documented midlatitude processes (e.g., *Appenzeller et al.* [1996] and *Reid and Vaughn* [1991] in the stratosphere, and *Cooper et al.* [1998] in the upper troposphere), evidence of seasonal, zonal, and hemispheric asymmetries in meridional transport were not clearly revealed in the subtropics until *Trepte et al.* [1993] investigated the 1-year poleward dispersion of volcanic aerosols from the 1991 Mount Pinatubo eruption. In particular, they interpreted the transport regime observed at 25 km altitude as being associated with planetary waves interacting with the QBO. The role of the QBO was further emphasized by *Chen et al.* [1994], and later *Shuckburg et al.* [2001] suggested that strong mixing observed in the subtropics during the westerly phase of the QBO was not only due to extratropical planetary wave propagation and breaking, but also to barotropic instabilities initiated within the tropical westerlies. Finally, *Orsolini and Grant* [2000] recently suggested that not only the QBO but also midlatitude large-scale stratospheric vortices could cause significant transport and mixing into and out of the tropics. The numerous physical processes mentioned above illustrate the high complexity of transport and mixing in the subtropical stratosphere. In the second part of this paper we will briefly review the possible relationships between ozone variability and circulation in the subtropical stratosphere by exploring the correlation between the ozone measured by lidar above MLO and TMF, and the dynamical and geographical origin of the air masses sampled.

[5] A small subset of the available JPL lidar data (summer 2002) has been used in this paper to perform the first in a series of transport studies, the ultimate goal of which is to identify the role of the upper tropospheric and stratospheric circulation over the Pacific on the ozone variability as observed by lidar. After a brief review of the JPL lidar instruments and global meteorological data sets used (section 2), our results on the connection between the ozone variability locally observed by lidar, and the circulation over the Pacific region, will be twofold: (1) in the UTLS (section 3), it will be shown that specific RWB events near Hawaii are easily identified by the MLO lidar as periods of enhanced ozone, (2) in the stratosphere, it will be shown that for all isentropes between 340 and 1200 K except the 500–700 K region, a significant degree of correlation exists, even in summer, between the ozone variability

measured by lidar, and the origin of the air masses sampled (section 4).

2. Data Sets and Diagnostic Tools

2.1. JPL Lidar Instruments and ECMWF Meteorological Data

[6] Three differential absorption lidars (DIAL) have been developed at the Jet Propulsion Laboratory (JPL) to measure profiles of tropospheric ozone, stratospheric ozone, aerosols, and middle atmospheric temperature. The Rayleigh DIAL technique used by these lidars for ozone measurement has been widely described in the literature [e.g., *Grant*, 1989]. Briefly, two laser beams are emitted into the atmosphere at two different wavelengths (one weakly absorbed by ozone, and the other one nonabsorbed). The laser light is Rayleigh-backscattered by the air molecules. The returning photons are collected by a telescope and sampled with time, i.e., geometric altitude. After various corrections, ozone number density is retrieved from the signals measured at both wavelengths. In the presence of aerosols, vibrational Raman scattering by atmospheric nitrogen molecules can be used when Rayleigh measurements are no longer possible due to the contamination by Mie scattering.

[7] The original JPL DIAL system has been operating since 1988 at the Table Mountain Facility in California (TMF, 34.4°N, 118.8°W) [*McDermid et al.*, 1990] and has measured more than 2000 cloud-free, aerosol-free, nighttime stratospheric ozone profiles (16–55 km max range). In 1991–1993 an improved system, notably by implementation of Raman channels, was developed and installed at the NDSC primary station of Mauna Loa Observatory in Hawaii (MLO, 19.5°N, 155.6°W), allowing ozone measurements from well below the tropopause to 55 km [*McDermid et al.*, 1995]. About 2000 ozone profiles have been routinely obtained by this system since 1993. Finally in 1999 a newly reconfigured system was deployed at TMF to measure tropospheric ozone up to 20 km [*McDermid et al.*, 2002]. A recent improvement in the tropospheric ozone retrieval that additionally uses one channel of the colocated stratospheric ozone system permits a single ozone profile to be retrieved from 4 km to 30 km altitude and, if combined with the 18–55 km stratospheric ozone profile, allows a single ozone profile to be retrieved over a 4–55 km altitude range. The instrumental vertical resolution is 300 m for MLO and the TMF stratospheric system, and 75 m for the TMF tropospheric system. Following the NDSC guidelines, the JPL lidars typically operate 2 hours per night, 4 to 5 nights a week, and the results are archived on a monthly basis at the NDSC data archive (see http://www.ndsc.ws for details). A lidar climatology of stratospheric ozone at TMF and MLO [*Leblanc and McDermid*, 2000], and an early study of the Quasibiennial Oscillation (QBO) at MLO [*Leblanc and McDermid*, 2001] have been published. The data set used in the current study extends from 1 June to 30 September 2002, which results in 55 stratospheric ozone profiles measured at MLO, 50 stratospheric and 28 tropospheric ozone profiles measured at TMF.

[8] The ozone number density as a function of geometric altitude was converted into mixing ratio by using, for MLO, the local air density profiles obtained from the twice-daily Hilo (155.1W, 19.7N) radio soundings, and for TMF, by using the NCEP operational analysis interpolated at the TMF location. The mixing ratio profiles were then interpolated vertically onto 55 isentropic levels using global ECMWF analyses. These data, accessible to the NDSC participants at the Norwegian Institute for Air Research (NILU) database (http://www.nilu.no), consist of 6-hour interval operational winds, temperature, and geopotential height analyses interpolated from the initial T106-60 levels ECMWF model grid onto 55 isentropic levels (300 to 2000 K, 5 K in the UTLS), with a 1.125° × 1.125° horizontal resolution. The model has undergone several improvements over the past few years, especially in March 1999 when a new 4-D variational scheme was introduced [*Rabier et al.*, 2000; *Mahfouf and Rabier*, 2000; *Simmons and Hollingsworth*, 2002, and references therein].

[9] The IPV was calculated from the isentropic ECMWF horizontal winds, temperature, and geopotential height. In this paper, unless otherwise specified we will always use the terms "vertical" and "horizontal" in the isentropic sense, i.e., "vertical" will mean "cross-isentropic," and "horizontal" will mean "onto a specific isentropic surface." PV units (10^{-6} K.m^2.kg^{-1}.s^{-1}) will always be used unless otherwise specified, and the "modified IPV" (MPV) introduced by *Lait* [1994], i.e., the IPV multiplied by $(\theta/\theta_0)^{-9/2}$, with θ_0 = 350 K will be used when the strong "vertical" dependence of Ertel's PV needs to be eliminated (for example when representing vertical cross sections of PV without encountering scaling problems due to the exponential increase of Ertel's PV with altitude).

2.2. High-Resolution IPV Advection Model Mimosa

[10] The Modèle Isentrope du transport Méso-échelle de l'Ozone Stratosphérique par Advection (MIMOSA) was originally developed at Service d'Aéronomie du CNRS in the frame of the European project METRO (Meridional Transport of Ozone in the lower stratosphere) in order to capture and quantify the filamentary structures passing over Europe in winter and spring and to assess the importance of such structures in the irreversible transport of polar air into midlatitudes [*Hauchecorne et al.*, 2002]. In an idealized adiabatic, frictionless atmosphere, IPV is a conserved tracer with a zonally mean positive latitudinal gradient throughout the stratosphere (i.e., poleward in the Northern Hemisphere). Because of the variation with height of the latitudinal gradient of ozone (positive, i.e., poleward, in the lower stratosphere and negative in the upper stratosphere) a positive correlation with PV in the lower stratosphere and negative correlation in the upper stratosphere is expected.

[11] The coarse grid analyzed isentropic winds and IPV extracted from ECMWF are input to MIMOSA where they are interpolated onto an azimuthal equidistant projection grid with a very fine resolution of three points per degree. The IPV is advected using a 1-hour elementary time step and re-interpolated onto a regular longitude-latitude grid. In the present study, the output longitude-latitude grid has been kept identical to the model grid, i.e., 3 points per degree in latitude and longitude. The combined use of a proper interpolation and re-gridding scheme with a particular model grid produces numerical diffusion that matches closely the actual horizontal diffusion, as estimated from observations [*Hauchecorne et al.*, 2002]. However,

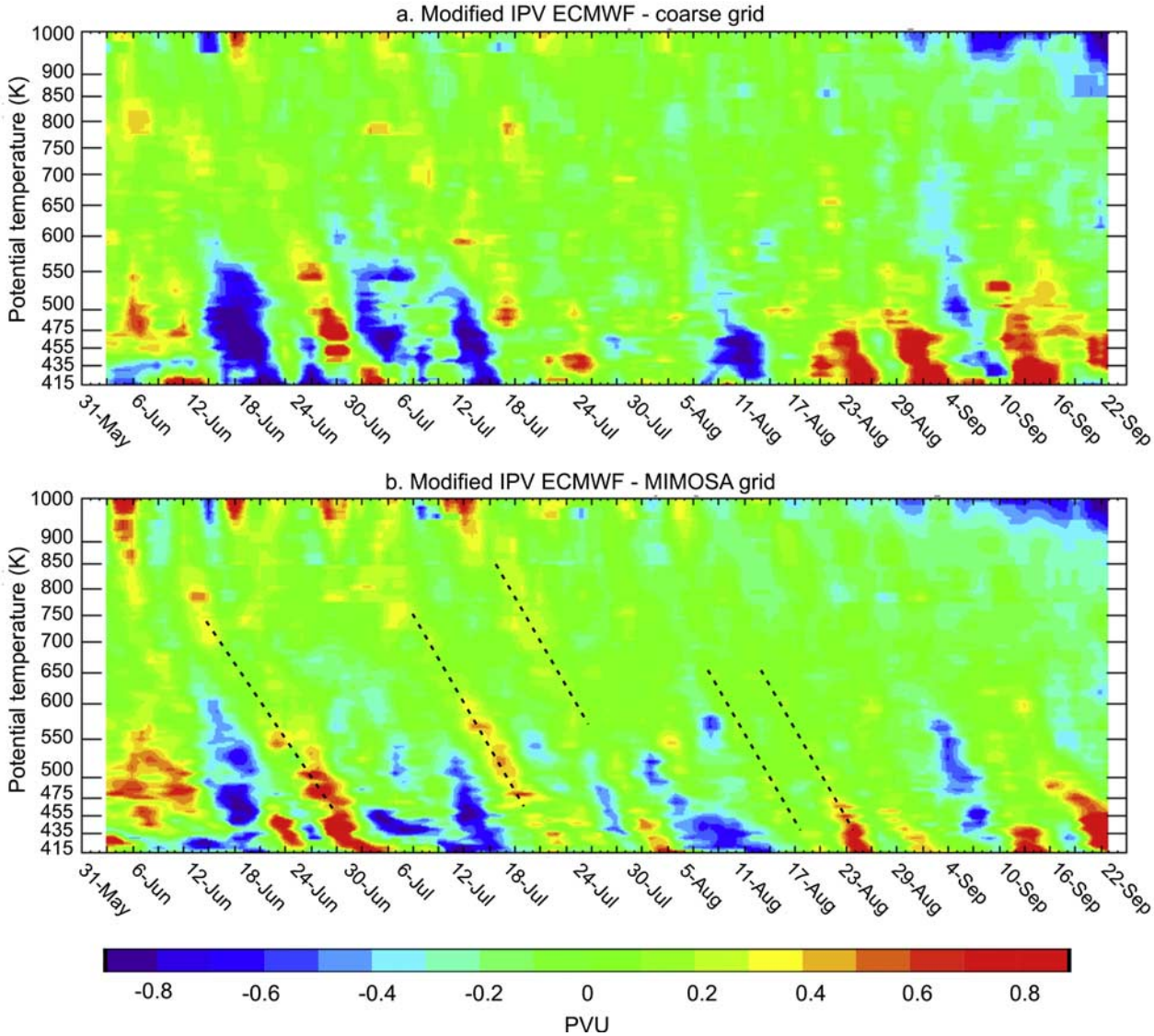

Figure 1. Modified IPV anomalies above MLO as computed from (a) the ECMWF coarse grid and (b) from MIMOSA.

the numerical diffusion obtained for an optimized use of MIMOSA in the lower stratosphere is generally not suitable for use in the uppermost stratosphere or in the mid and low troposphere. To account for diabatic processes, the high-resolution IPV is relaxed with a ten-day relaxation constant toward the coarse grid IPV extracted from ECMWF. This relaxation technique allows the model to run over several weeks or months with, for example, the diabatic descent inside the winter polar vortex implicitly reproduced. The technique used in MIMOSA (smoothed difference between PV from meteorological analysis and advected PV) assumes that diabatic processes are slow and homogenous at scale of a few hundreds of kilometers. This is true in the upper troposphere outside areas with deep convection reaching the tropopause, which are quite rare according to *Gettelman et al.* [2002], and mainly located above tropical continental areas (South America, Africa and Indonesia). Outside of convective areas, the motion of air parcels across isentropic surfaces is controlled by radiative processes (net heating or net cooling), which are very limited above 320 K (much less than 1 K/day), due to low concentration of potential absorbers of solar flux (ozone and water vapor).

[12] Fifty-three MIMOSA parallel runs (corresponding to 53 isentropic levels from 320 K to 1500 K) were initialized on 1 May 2002, and run continuously for 5 months. It takes about 10 to 15 days for the model to develop filamentary structures to full scale, and so by 15 May, the IPV outputs from MIMOSA could be compared to those extracted from the coarse grids and correlated with the ozone mixing ratios measured by the JPL lidars. Figure 1 shows a comparison of the time-height cross sections of MPV anomalies through the summer 2002 computed from the original ECMWF coarse grid (Figure 1a), and output from MIMOSA (Figure 1b). The anomalies (in PVU) are calculated here as deviations from the seasonal (4-month) mean. Coherent IPV fluctuations with an apparent downward propagation are clearly produced by the high-resolution model (denoted by black dotted curves in Figure 1b). These fluctuations, which are most likely due to differential advection of planetary wave induced perturbations, are hardly identifi-

able in the coarse grid data. The vertical coherency of the structures seen in Figure 1b, as compared to Figure1a, thus suggests that using a high-resolution model like MIMOSA helps filter noisy features probably caused by the coarser horizontal resolution of the ECMWF original grid. In MIMOSA, structures like streamers and filaments are fully resolved, and in regions of strong PV gradients, MIMOSA will better capture details in connection with these features, though it does not eliminate completely all noisy features. Smoother features in MIMOSA will also be observed later in this paper, when considering the latitude-height cross section of MPV.

2.3. Backward Trajectories

[13] Ten-day isentropic backward trajectories were computed to complement the use of MIMOSA. A few theoretical studies [e.g., *Stohl*, 1998, and references therein] have reviewed the accuracy of different types of trajectories, their resolutions, and numerical schemes. Our choice of model grid, horizontal resolution, and time step scheme were constrained by the compromise between computational requirements (CPU time) and results from previous reports. We have calculated trajectories of single parcels that end at the exact position of the JPL lidars, and at the exact time of the lidar measurements. *Knudsen et al.* [2001] among others have shown that the accuracy of analyzed winds was probably the major source of error in trajectory calculation as compared to errors due to horizontal resolution, numerical scheme, or time step. In order to evaluate the errors due to the use of ECMWF winds, trajectories were also calculated using the winds from the NCEP-NCAR reanalysis Project [*Kalnay et al.*, 1996], and compared to those computed from ECMWF. Though a number of trajectories showed slightly different paths (not shown), the main results presented in this paper are not affected, i.e., the conclusions are identical using either NCEP or ECMWF data sets. The wind horizontal resolution proved to have little influence on the 10-day trajectories. Using the ECMWF winds at twice-coarser resolution (every other grid point), *Hauchecorne et al.* [2002] found no difference in the position of fine PV structures with those obtained using the ECMWF original grid, which implies no difference in the trajectories. *Stohl* [1998], *Stohl and Seibert* [1998], and *Knudsen et al.* [2001] all found that time resolution of the analyzed winds becomes a concern only if using intervals exceeding 12-hours, which is twice as long as the 6-hour interval used here. For the results shown, the 10-day backward trajectories were calculated starting at each lidar measurement between 1 June and 30 September 2002 and for each available isentropic level, leading to a total of more than 5000 backward trajectories. Various air parcel properties along each trajectory, such as PV, equivalent latitude, "vertical" distance from the tropopause, etc., were calculated and compared to the parcel "instantaneous" ozone content as measured by lidar.

3. Ozone-PV Relationship Above MLO Near the Tropopause

3.1. Ozone and IPV Anomalies in the UTLS

[14] Figure 2 shows the deseasonalized MPV (in PVU) time-height cross sections at MLO in the tropopause region through the summer 2002, output from MIMOSA (Figures 2a and 2b) and the corresponding time-height cross section of deseasonalized ozone mixing ratio (in ppmv) measured by lidar (c). The time series at each altitude have been deseasonalized by applying a least-square 2nd degree polynomial fit to the 4-month series, then calculating the deviations from this fit. Note that, due to the large intra-seasonal variability relative to the seasonal trend, the deseasonalized series for all altitudes between 300–475 K yield very similar results to those using the deviations from the seasonal mean. In Figure 2a the polynomial fit has been calculated using MIMOSA MPV outputs every 6 hours (no data gap), while in Figure 2b, the fit has been calculated using only the values of the MIMOSA IPV outputs whose dates/times coincided with lidar measurements (i.e., including data gaps). In this way, the effect of irregular lidar data sampling is directly observable by comparing Figures 2a and 2b, and the correlation between MPV and ozone mixing ratio is directly observable by comparing Figures 2b and 2c. The approximate vertical locations of the WMO (black) and dynamical (purple) tropopauses calculated from the coarse grid data are superimposed. The WMO tropopause is based on the vertical position and persistence of a threshold temperature lapse rate [*World Meteorological Organization* (*WMO*), 1957]. The dynamical tropopause has been chosen here to be the altitude (or more precisely the isentropic level) at which the vertical gradient of IPV maximizes in a layer situated between the midtroposphere and the midstratosphere. It is defined as the lower isentropic level at which $\partial(\mathrm{IPV})/\partial\theta$ maximizes, with values above the threshold value of 0.1 PVU/K. This threshold value is not critical and can be chosen up to 0.15 PVU/K because this range of values occurs in a well defined layer of abrupt transition between low values (in the troposphere) and high values in the layer just above. We have preferred this definition of the dynamical tropopause to the more common definition based on a constant PV value due to the limited use of a single PV value when considering a large range of latitudes, as it is the case here.

[15] Around the tropopause (350–380 K), high variability on timescales of a few days can be observed during the first part of the summer. This is the common signature of Rossby wave fluctuations and other synoptic disturbances that appear stronger in June and early July, but still remain during most of the summer. The quietest period occurs between 27 July and 16 August, and can be considered as the "core" of the summer 2002 season with the persistence of low PV, and low ozone mixing ratios, and where most of the air parcels sampled between 340 and 370 K remain below both the WMO and dynamical tropopauses. Inspection of synoptic maps of PV on the 330–360 K surfaces showed that high-PV air masses remained well north of the Hawaiian Islands during this period. Throughout the summer the positive correlation between MPV and ozone mixing ratio is clearly characterized by collocated regions of same sign anomalies (Figures 2b and 2c), showing that the PV-ozone analogy near the tropopause and in the lowermost stratosphere still stands strongly during the relatively quiet well-mixed lower stratospheric summer regime.

[16] A remarkable pattern is revealed when inspecting the 10-day backward trajectories at 350 K of the air parcels

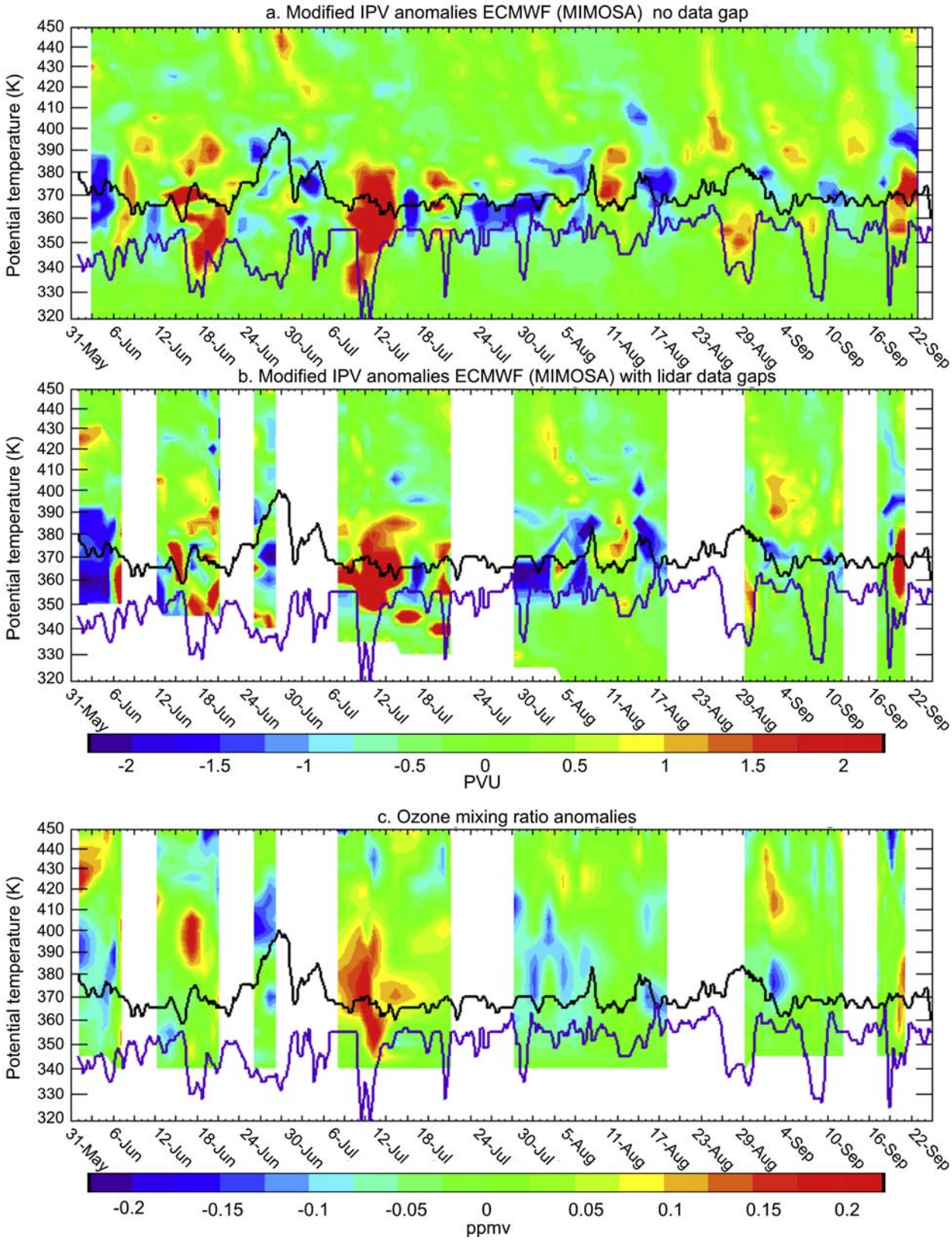

Figure 2. (a and b) Altitude-time cross sections of deseasonalized modified IPV computed from ECMWF (MIMOSA outputs) above MLO and (c) deseasonalized ozone mixing ratio measured by the MLO lidar. See text for details on the difference between Figures 2a and 2b, and on the way the times series were deseasonalized. The black and purple solid lines indicate the WMO and dynamical tropopauses respectively.

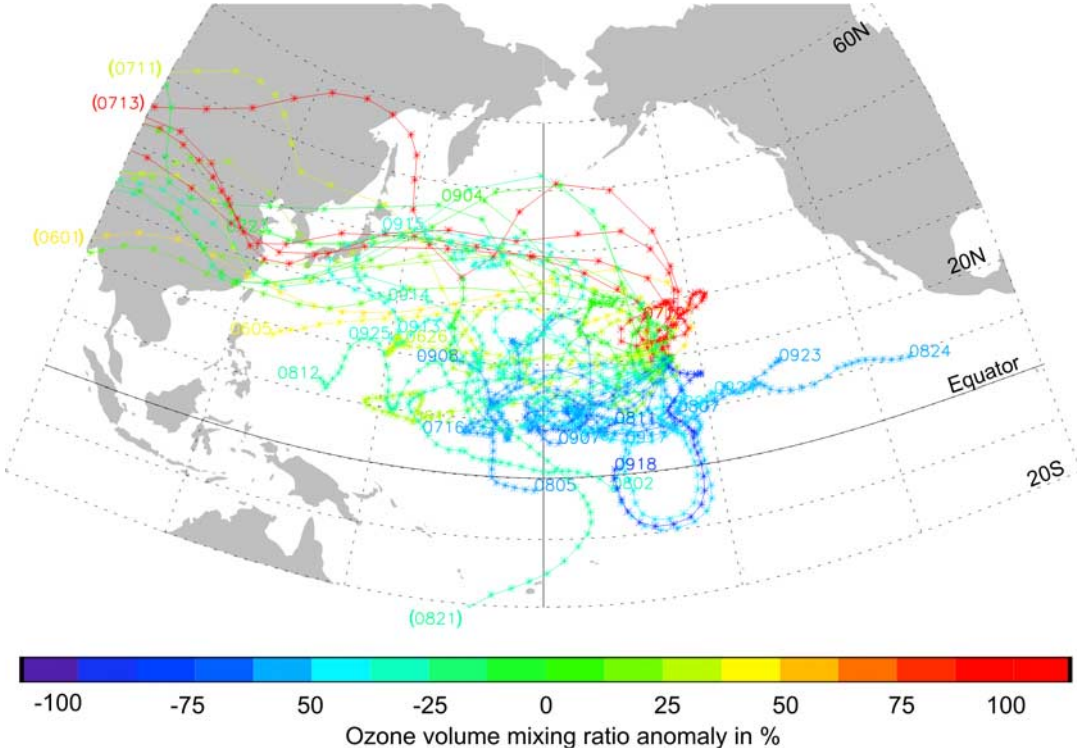

Figure 3. Ten-day backward trajectories at 350 K of the 51 air parcels sampled by lidar at MLO between 1 June and 30 September 2002. Each trajectory is color-coded by the deseasonalized ozone mixing ratio as measured by lidar (see text for details). Each parcel is tagged at its starting point by the date of lidar measurement (ending point). A few trajectories that started outside the plotting area (including that ending at MLO on 13 July 2002) have their tag between parentheses just outside the plotting area (not the actual location of their starting points).

sampled by lidar during the entire summer (Figure 3). In this figure, each trajectory is color-coded by the parcel's ozone mixing ratio anomalies shown in Figure 2c. Almost all of the parcels sampled that contained high ozone mixing ratios at 350 K followed the same route prior to passing over Hawaii, specifically being advected clockwise around the northern and eastern side of a high pressure cell located just northwest of the islands. In contrast, almost all of the parcels sampled that contained low ozone concentrations at this level originated over the tropical central Pacific Ocean.

[17] As shown in the next section when considering the particular event of 12–16 July 2002, the maximum variability observed between the 350 and 370 K levels is typified by alternate periods of tropospheric and stratospheric regimes at a given isentropic level. The positive anomalies correspond to the passing of lower stratospheric midlatitude air masses, when the tropopause in the North Pacific region is meridionally displaced southward of Hawaii by Rossby waves (see the temperature profile for 13 July in Figure 1c resembling that of midlatitudes). The negative anomalies correspond to periods of upper tropospheric tropical regimes, when the tropopause in the tropical Pacific region is meridionally displaced northward of Hawaii (see the temperature profiles for 9 and 16 July in Figure 4c more typical of the tropics). As shown in Figure 2, during each stratospheric episode the dynamical tropopause potential temperature decreases significantly (up to 20 K), while the WMO tropopause potential temperature remains weakly affected. Several "stratospheric events" can be observed, the most significant ones being around 7 June, 13 July, and 22 September. Most of the time the Rossby waves have not reached a critical amplitude, or critical surface, and are seen as large-scale gentle undulations of IPV that extend into the subtropical central Pacific. Occasionally however, these waves reach saturation and their breaking is manifested on IPV maps by the overturning of the PV contours leading to isentropic transport across the tropopause [*Thorncroft et al.*, 1993]. The specific RWB event of 13 July over Hawaii is now outlined.

3.2. Case Study of a Rossby Wave Breaking Event Over MLO

[18] Around 12–14 July, the ozone mixing ratio anomaly measured by lidar near the tropopause exceeded 100% (Figure 2c). Figure 4a shows the corresponding high-resolution ozone number density profile measured by the JPL lidar at MLO (12 July), and Figure 4b the derived isentropic mixing ratio profile. Similar ozone-enhanced layers are frequently observed on the JPL lidar profiles, not only at MLO but also TMF. The evolution of the IPV field output from MIMOSA on the 350 K surface between 9 and 16 July 2002 is depicted in Figures 5a–5f. The dates and times have been chosen to coincide with the MLO lidar measurements. The IPV is plotted with color contours and the horizontal wind speed is superimposed with white contour lines. The sharp IPV transition from green to red located mainly north

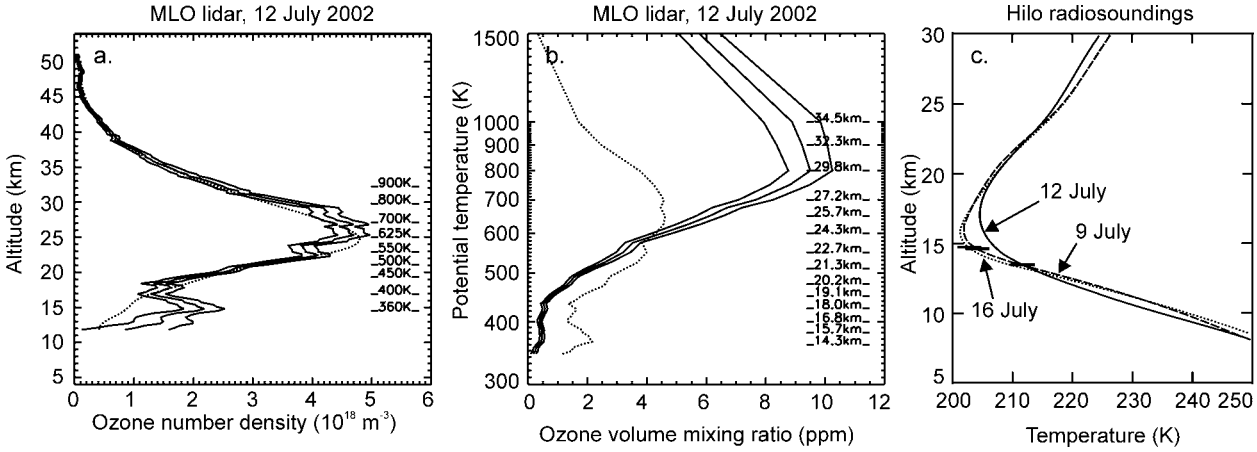

Figure 4. (a) Ozone number density profile measured by the JPL lidar at MLO on 12 July 2002. The dotted curve depicts the zonal mean UARS climatology for that day of year. The approximate isentropic levels are included where simultaneous lidar temperature measurements were available. (b) Isentropic ozone volume mixing ratio (in ppm) derived from the profile shown in Figure 4a. The dotted curve indicates the isentropic ozone number density (in 10^{18} molecules m^{-3}). The approximate geometric altitudes are indicated. (c) Temperature profiles measured by the Hilo (155.1°W, 19.7°N) radio soundings on 9, 12, and 16 July 2002. Three horizontal segments indicate the WMO tropopause for each profile shown.

of 50°N, colocated with strong horizontal winds, delineates the intersection of the tropopause with the 350 K isentrope and the location of the tropopause jet. Until 12 July, at this level the MLO lidar sampled air parcels located in the vicinity of the subtropical jet far south of the region where the tropopause intersects that isentrope. The air sampled at this altitude was of tropical upper tropospheric origin, characterized by low ozone mixing ratio, low IPV, and a high (on a geometric altitude sense) WMO tropopause (15 km), with a strong lapse rate below (almost typical of tropical temperature profiles, see Figure 4c, dashed curve for 9 July). By 13 July, following strong deformation by Rossby waves, an upper level trough formed in the north central Pacific and slid southwards to the Hawaiian Islands, rolling up clockwise around a high pressure cell located northwest of Hawaii. On 12 July at this level, the MLO lidar sampled lower stratospheric air (high ozone values, high IPV, and a lower WMO tropopause (13 km) with a weaker lapse rate more typical of midlatitudes, see Figure 4c, solid curve). This air was transported southward from the Aleutian region by the tropopause jet tilting along the western edge of this extended trough. On this date, the subtropical jet shifted south of the Hawaiian Islands, and the elongation of the trough eventually led to the development of a cutoff low system that formed over Hawaii, and was later advected eastward, following the mean zonal flow. The cutoff system, initially circular (not shown), quickly became elongated as seen in Figure 5f. After the passing of the cutoff over the island (16 July), the lidar again sampled upper tropospheric tropical air with similar characteristics than that described for 9 July (dotted temperature profile in Figure 4c). Note that on Figure 4c, the WMO tropopause elevation (i.e., geometric altitude) decreases at the time of the passing trough, but its isentropic level did not vary significantly as could be seen in Figure 2. The evolution of this particular RWB event is typical, and follows remarkably well the behavior of the LC1-type RWB event modeled by *Thorncroft et al.* [1993], including the upstream tilting of the high PV tongue and the elongated shape of the newly formed cutoff low. This cutoff low system never reconnected with the main high PV reservoir (not shown), implying likely net isentropic transport and mixing of high-latitude lower stratospheric air into the subtropical upper troposphere.

[19] Figure 6 shows, for 13 July, the latitude-height cross section of MPV along the meridian intersecting MLO, calculated from the coarse ECMWF model grid (Figure 6a) on the one hand, and output from MIMOSA (Figure 6b) on the other. As for Figure 2, the white and purple curves depict the WMO and dynamical tropopause levels as calculated on the coarse grid between 10° and 60° latitude. As expected, finer details are captured by MIMOSA than by the coarse grid model. Interestingly, contours appear smoother for MIMOSA than for the coarse grid. Knowing that MIMOSA advects IPV independently for each isentropic level, this illustrates the remarkable consistency (already shown from Figure 2) between isentropic levels, and the suitability of using a high-resolution advection model with a re-gridding technique in parallel runs on separate levels. In Figure 6b, the 13 July stratospheric intrusion into the tropical upper troposphere above MLO appears as a coherent body of high IPV, extending southward and downward from about 390 K at 32°N to 350 K at 20°N. In contrast, the coarse grid model (Figure 6a) does not reproduce such a coherent structure, but instead, several weakly coherent spots of high MPV that hardly extend into the tropical troposphere.

[20] Two other interesting features in Figure 6 are noteworthy, though they are not directly related to our current study. First, an equatorial isentropic transport barrier characterized by tight, nearly vertical MPV contours is clearly apparent between 380 and 450 K between 10°S and the equator. This barrier is not as sharp when considering the coarse grid. Though the concept of "transport barrier" has

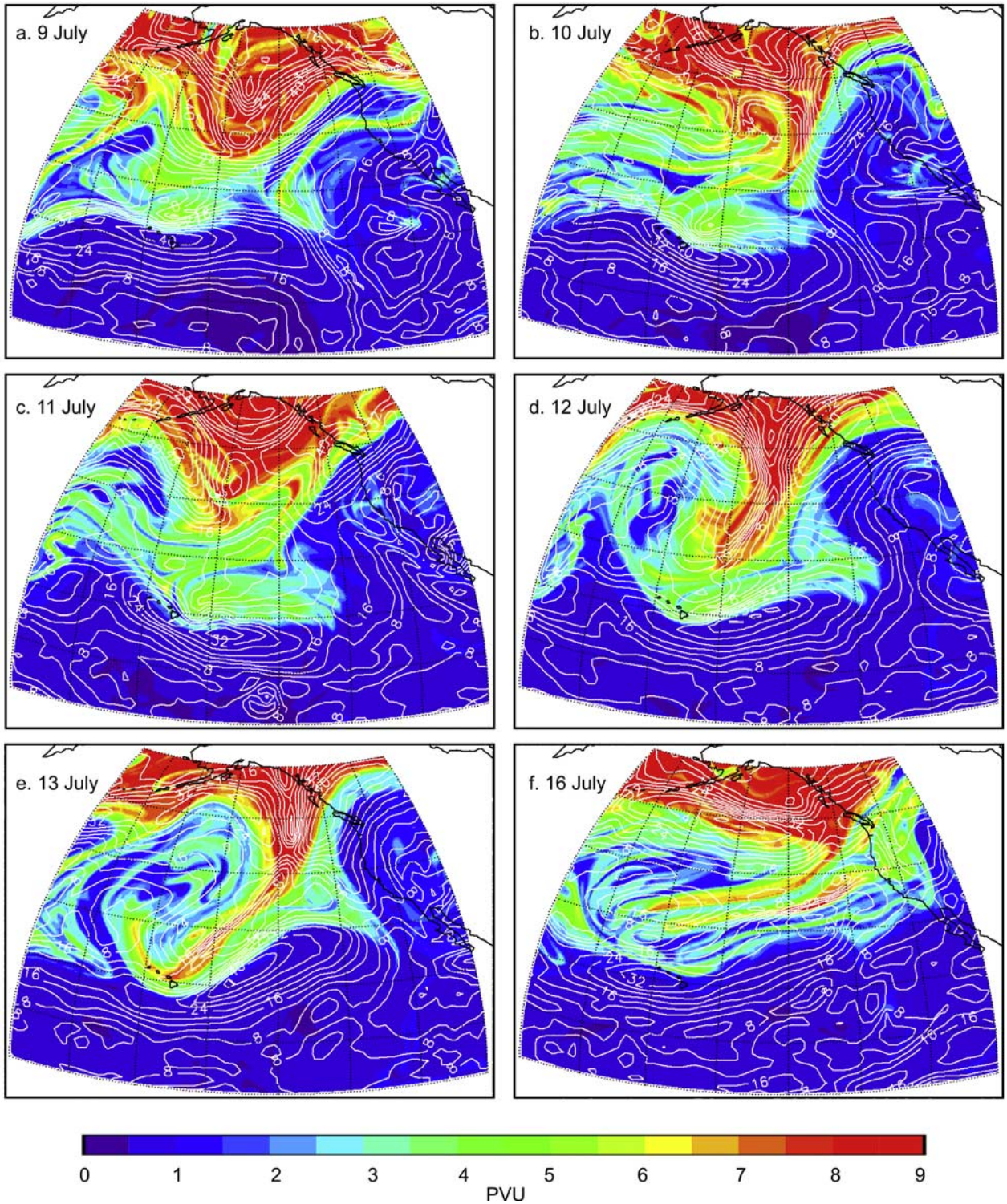

Figure 5. Isentropic maps of IPV output from MIMOSA IPV at 350 K on (a) 9, (b) 10, (c) 11, (d) 12, (e) 13, and (f) 16 July 2002. The wind speed (in m s^{-1}) is superimposed with white contour lines.

mostly been considered in the past in a climatological sense, this region of high PV gradient persisting for days (not shown) can be regarded here as an "instantaneous barrier," and therefore could be investigated in a similar manner as the polar vortex barrier has been many times (beyond the scope of the present work). The second interesting feature in Figure 6 is a massive intrusion of tropospheric tropical air into the southern midlatitude lowermost stratosphere (up to 400 K), well captured by MIMOSA, but mostly blurred by the coarse grid model. Note that the good spatial coherency of the MPV structures seen in Figure 6b (MIMOSA grid) compared to those seen in Figure 6a (coarse grid) was also

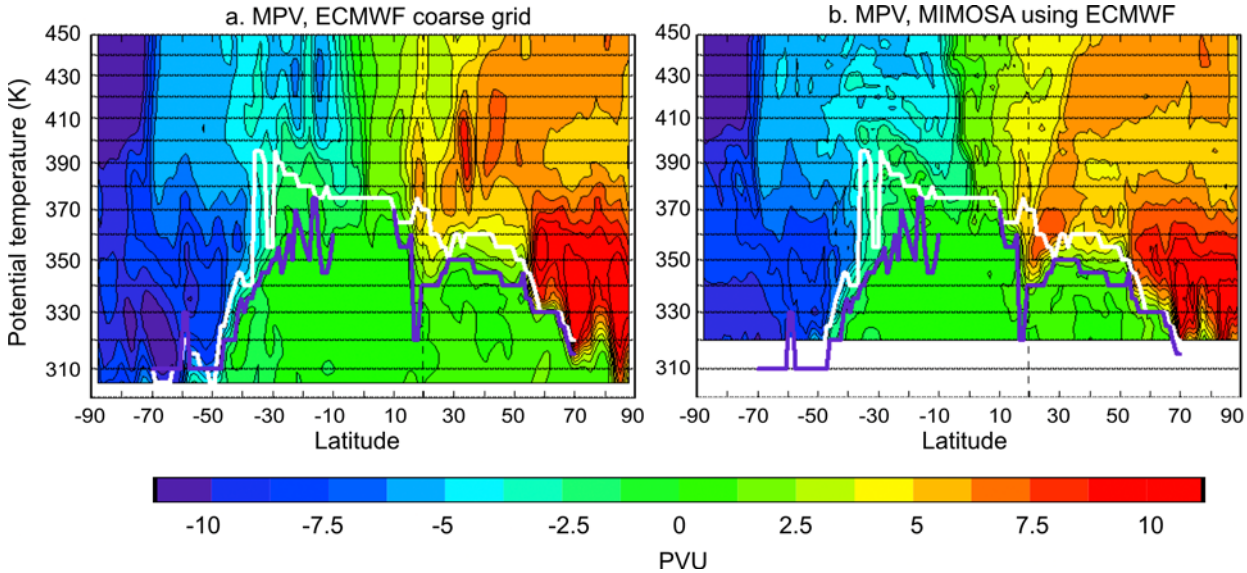

Figure 6. (a) Latitude-height cross section of modified IPV computed for 13 July 2002 0600 UT at the longitude of MLO from the ECMWF analysis on their original grid and (b) output from MIMOSA. The white and purple solid lines indicate the WMO and dynamical tropopauses respectively.

observed when using the winds and IPV from the NCEP reanalysis instead of ECMWF (not shown).

4. Stratospheric Ozone Measured by Lidar and Origin of the Air Masses Sampled

[21] In this section, we will show several "vertical" profiles of correlation coefficients between the ozone fluctuations measured by the MLO and TMF lidars, and the origin of the air parcels sampled. The "origin" is expressed here in terms of latitude, and equivalent latitude averaged along their 10-day backward trajectories. The equivalent latitude of a given PV contour (introduced by *Butchard and Remsberg* [1986], also named "vortex-following coordinate" by *Norton* [1994]) is the latitude of a circle surrounding the pole and having the same area as that PV contour. In winter it is a dynamical indicator of the strength of the polar vortex. In all seasons, it is a good indicator of the atmospheric reservoirs the air parcels belong to. These reservoirs are separated by "transport barriers." Reservoirs and barriers are not geographically fixed, i.e., their latitude/longitude vary with time, so that equivalent latitude helps characterize the origin of air parcels regardless of their meridional displacement.

[22] Throughout this section we will try to identify possible signatures connected with photochemical/radiative processes along the parcels' path. By photochemical/radiative processes, we mean "short-lived" (as compared to 10 days or longer) photochemical reactions or radiative effects that would induce changes in the ozone abundance of an air parcel during a traveling time of several days. We will assume that, on the average timescale of a few days, the ozone chemical net production rate is a simple function of local chemical composition and insolation (i.e., a simple function of geographical latitude in a zonally symmetric atmosphere). If photochemical/radiative processes remain weak while a parcel is traveling, its chemical composition will remain consistent with the mean composition of the reservoir it belongs to, regardless of its latitude change. If photochemical/radiative effects (which, if averaged over a few days, depend on the latitude only) are important enough to change the ozone abundance of a traveling air parcel, then the composition of this parcel will no longer be that of the reservoir it belongs to.

4.1. MLO

[23] Figures 7a–7d summarize, for levels between 350 and 1500 K, the magnitude, sign, and nature of the calculated correlation between the ozone fluctuations measured by lidar at MLO, and the origin of the air masses sampled. Figure 7a shows the correlation coefficient, as a function of potential temperature, between the ozone mixing ratio anomalies measured by lidar (calculated as deviations from the seasonal mean) and the latitude averaged along the 10-day isentropic backward trajectories ending above the lidar site at the time of the measurement (anomalies also calculated as deviations from the seasonal mean). The light shaded area delineates the region where the correlation coefficient values remain below the 95% level of statistical significance, and the dark shaded areas that below the 99% level. Asterisk symbols are displayed for each point of the curve above the 95% level. Figure 7b is similar to Figure 7a, but this time the ozone and latitude time series are deseasonalized, i.e., the anomalies are calculated as deviations from the 2nd degree polynomial representing the best fit of the data series over the 4-month period considered. Figures 7c and 7d (bottom) are similar to Figures 7a and 7b, respectively, but this time using the averaged equivalent latitude instead of the averaged latitude. Figures 7a–7d all together give a good overall picture of the significance, and possible sources of the observed correlations.

[24] Comparing the left and right figures helps identify which isentropic levels exhibit correlations that are purely intraseasonal, as opposed to correlations associated with either seasonal or interannual variations. For example, it is shown that, when studying the ozone-latitude correlations

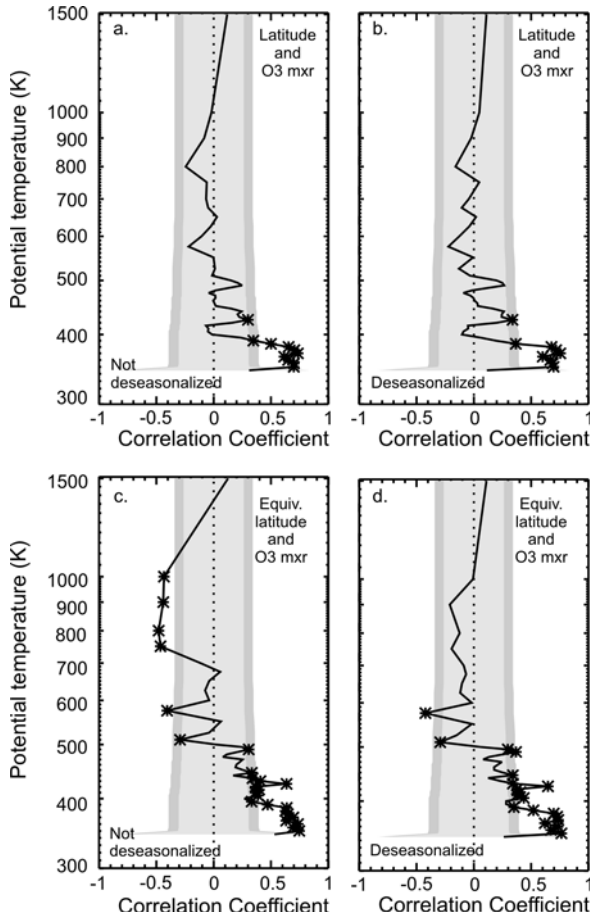

Figure 7. Correlation coefficient as a function of potential temperature, between the ozone mixing ratio anomalies measured throughout summer 2002 by the MLO lidar, and the latitude/equivalent latitude averaged along the 10-day backward trajectory of the air parcels sampled. (a and b) Latitude. (c and d) Equivalent latitude. In Figures 7a and 7c, anomalies are the deviations from seasonal average. In Figures 7b and 7d, time series are deseasonalized (see text for details). The light shaded area delimits the 95% statistical significance level, and the dark shaded areas the 99% level. The asterisks indicate calculated correlation coefficients with statistical significance above the 95% level.

(top plots of Figure 7), there is no difference whether considering the seasonal mean or the deseasonalized series. The only statistically significant correlation here lies in the lowermost stratosphere, and is the result of episodes of maximum ozone mixing ratios associated with air masses coming from higher latitudes, and minimum mixing ratios associated with air masses from lower latitudes, as mentioned earlier in this paper. The RWB event outlined in the previous section was an extreme example of such episodes. At altitudes of highest statistical significance (correlation coefficients greater than 0.5 between 350 and 400 K), there is an average 10-ppb (5%) positive ozone deviation per degree of latitude, which is 50% larger than the climatological meridional ozone gradient [see, e.g., *Fortuin and Kelder*, 1998].

[25] Using the assumption described in introduction of this section, comparing the top and bottom figures helps identify correlations possibly connected to purely dynamical (or more generally transport) processes, as opposed to purely photochemical/radiative processes, or mixed chemical/radiative transport processes. The identification of the possible role of one of these processes does not lie in the interpretation of the correlation observed on a single plot (e.g., equivalent latitude alone), but instead in the interpretation of the difference in the observed correlation between the top plot and the bottom plot. Above the UTLS, a significant increase of the correlation coefficients can be found between 400 and 450 K when considering the equivalent latitude (Figure 7, bottom) instead of the geographical latitude (Figure 7, top). This is an indication of a likely dominant role of transport over photochemical/radiative processes in the fluctuations of ozone observed at MLO in this range of altitudes. In this region the ozone mixing ratio measured by lidar varies in average by 20 ppb/degree equivalent latitude (4–5%), which is of the same order of magnitude as the climatological meridional ozone gradient in this range of altitudes and latitudes.

[26] Finally, by comparing the bottom-left and bottom-right plots in Figure 7 (equivalent latitude), it is shown that, besides the positive correlation in the lowermost stratosphere already pointed out for the geographical latitude, there are additional isentropic levels in the middle stratosphere with statistically significant negative correlations, not present when considering the geographical latitude. This would indicate that these are mainly associated with transport processes. The negative correlation at 500–600 K is present whether considering the deseasonalized series or not. By contrast, the negative correlation observed between 750 and 1000 K when considering the seasonal mean, fades away when considering the deseasonalized series. As shown later, it is in fact the result of a continuous increase of ozone (1.5 ppm), combined with a continuous decrease of the averaged equivalent latitude along the trajectories (8°) throughout the season.

4.2. TMF

[27] Figures 8a–8d are similar to Figures 7a–7d, but for TMF instead of MLO. One substantial difference to MLO is that there is very little change from one plot to another. The small variations between the top and bottom plots indicate that we cannot extract any effect due to transport alone (i.e., photochemical/radiative processes may as well be contributing, since geographical and equivalent latitudes yield identical results). The small variations between the left and right plots indicate that there is no effect solely related to the seasonal or interannual variability, as was the case for MLO in the range 800–1000 K. Therefore the statistically significant positive correlation between 400 and 500 K (2% or 20 ppb per degree of latitude), and negative correlation between 650 and 800 K (2.6% or 0.2 ppm per degree of latitude), both being twice as large as the climatological meridional gradient at these altitudes, can fully be explained in terms of the origin and/or path of the air masses sampled, but we cannot say at this point if the origin of the correlation is dynamical or photochemical/radiative. One flaw of the present latitude/equivalent latitude analysis is the lack of robustness of the equivalent latitude diagnostic in summer

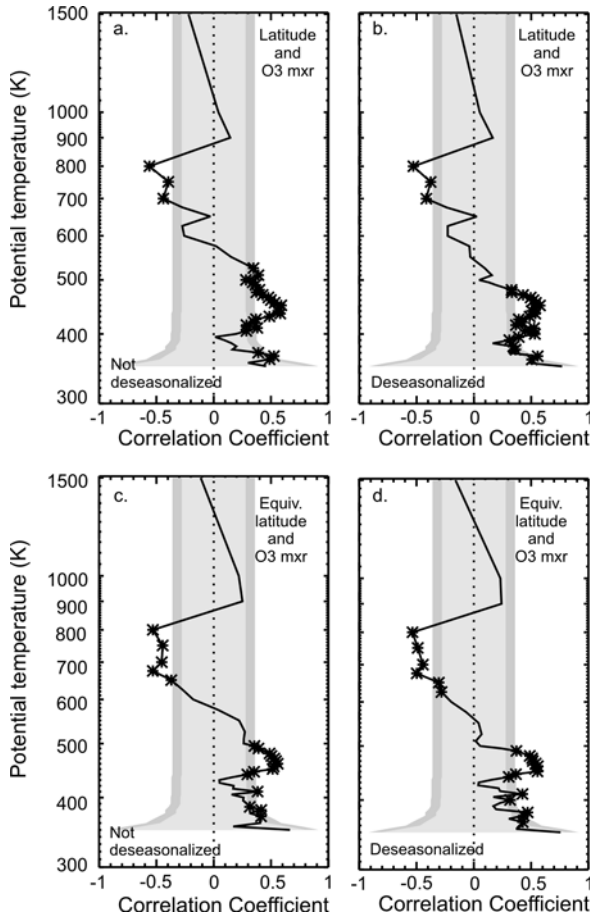

Figure 8. Same as Figure 7, but for TMF instead of MLO.

to identify processes of dynamical origin, due to the well-mixed character of the lower stratosphere compared to winter, where a clear boundary usually exists between the polar vortex, and the surf zone. This could explain why latitude and equivalent latitude exhibit a similar correlation pattern with ozone mixing ratio in the TMF case.

[28] The above results for both TMF and MLO are corroborated by inspecting Figures 7–11, which show three representative examples of time series, and scatterplots, of the ozone mixing ratios measured by lidar, and equivalent latitudes of the air masses sampled (at 800 K above MLO, and 675 K and 465 K above TMF respectively). On the time series plots, the horizontal dotted line indicates the seasonal mean, and the solid curve indicates the 2nd degree polynomial fit used to deseasonalize the series. The scatterplots show the deseasonalized anomalies, with the corresponding regression curve and correlation coefficient. The TMF time series at 465 K exhibits a much larger day-to-day variability than that of TMF and MLO above, relative to the seasonal trend, and the deviations from the seasonal mean, and that from the polynomial fit are of the same order of magnitude. This explains why considering deviations from the seasonal mean, or considering deseasonalized data, bear nearly identical results in this case. On the other hand, the MLO time series at 800 K exhibits a larger seasonal trend than intraseasonal variability. In fact, inspection of the IPV evolution between the summer 2002 and fall 2003 (not shown) revealed the presence of a strong QBO signal superimposed to the annual cycle, leading to maximum negative PV anomalies in fall 2002 (leading in our case to low equivalent latitudes at the end of summer 2002), and maximum positive PV anomalies in summer 2003. The negative correlation (−3% or −0.28 ppmv per degree of latitude) observed at MLO around 800–1000 K is therefore due to the combined effect of the QBO and the seasonal cycle, and has apparently no connection with intraseasonal variability.

5. Concluding Remarks

[29] The aim of this paper was to demonstrate that even in the weakly dynamically disturbed, well-mixed, summer stratosphere (summer 2002), signatures of correlation between ozone locally measured by lidar and dynamical proxies such as PV and equivalent latitude were widely observed. Though the results remain preliminary, they indicate that an extensive all seasons multiyear study should unveil many aspects of the possible connection between the stratospheric circulation in the subtropical northern Pacific region, and the stratospheric ozone variability observed by the JPL lidars at MLO and TMF.

[30] Figures 7 and 8, showing the latitude-ozone correlation coefficient as a function of potential temperature, confirmed the statistically significant positive correlation between ozone and equivalent latitude below 500 K, and negative correlation above. For TMF, this height dependence was found to be very similar to that calculated for midlatitudes by *Calisesi et al.* [2001].

[31] In the UTLS, the short 4-month period investigated here was adequate to point out the significant variability, even in summer, of the subtropical circulation and its local impact on ozone. In particular, the signature of Rossby wave breaking (RWB) events can easily be identified as high PV intrusions over the Hawaiian Islands associated

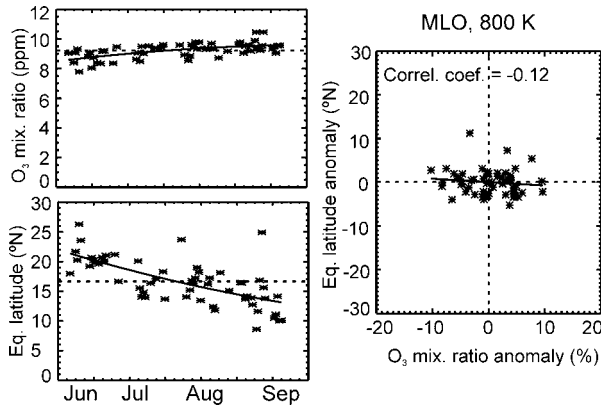

Figure 9. (top left) Time series at 800 K of the ozone mixing ratio measured by the MLO lidar, (bottom left) equivalent latitude averaged along the trajectory of the air parcels sampled, and (right) correlation between the two deseasonalized time series. See text for details. The dotted horizontal lines on the left plots indicate the seasonal mean, and the solid curves indicate the 2nd degree polynomial used to deseasonalize the data. The solid curve on the right plot indicates the regression slope. The corresponding correlation coefficient is also indicated.

with high values of ozone measured by the MLO lidar. The event of 13 July 2002 was briefly described in section 4, showing a typical LC1 type of breaking event as defined by *Thorncroft et al.* [1993]. *Postel and Hitchman* [1999] studied the frequency of RWB events on the 350 K surface, and found a strong seasonal cycle, with a summer maximum over the Pacific that coincides with that of Chen's STE calculations [*Chen*, 1995]. Additionally, *Waugh and Polvani* [2000] and *Waugh and Funatsu* [2003] noted a significant interannual variability characterized by reduced RWB in warm ENSO years (El Nino and the Southern Oscillation) as compared to cold ENSO years or climatological years. *Leblanc and McDermid* [2001] also observed lower ozone anomalies during the warm 1997/1998 ENSO, anomalies that temporarily obscured the observed ozone QBO signature below 25 km altitude. Therefore a systematic multiyear study of the ozone-PV correlations near the tropopause over Hawaii at all seasons, and their connection to RWB, should contribute to a better quantification and understanding of such events in the future, and their role in the ozone variability observed by the MLO lidar.

[32] Above the UTLS, statistically significant positive correlation between ozone and the equivalent latitude averaged along the trajectory of the air masses sampled, can be found up to 470 K for both TMF and MLO, and negative correlation can be found in the 675–800 K altitude range for TMF, and 750–1000 K range for MLO. The altitude dependence of the correlation coefficients for TMF (Figure 8) is very similar to that already observed by *Calisesi et al.* [2001] for summer and winter midlatitudes. However, the use of the geographical latitude on the one hand, and equivalent latitude in the other, showed two different results for MLO and TMF above 700 K. For TMF there was no apparent change in the equivalent latitude-ozone correlation aspect when considering either the deviations from the seasonal mean or the deseasonalized time series. For MLO the equivalent latitude-ozone correlation was well marked when considering the deviations from the seasonal means, but mostly absent when considering the deseasonalized data. The observed seasonal increase of ozone at this altitude above MLO throughout the summer 2002 was in fact accompanied by a seasonal decay of the equivalent latitude (Figures 9a–9b), decay that originated in the combined effect of the annual cycle and QBO on the Northern Hemisphere circulation.

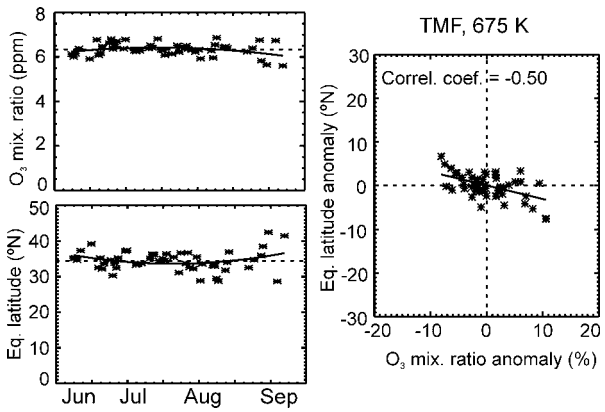

Figure 10. Same as Figure 9, but for TMF at 675 K.

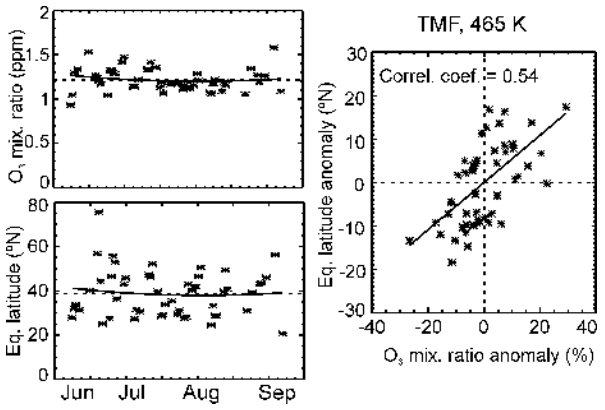

Figure 11. Same as Figure 9, but for TMF at 465 K.

[33] The work described in this paper using global meteorological fields from ECMWF has also been done using the NCEP reanalysis. When considering the original (coarse) grids, large meteorological features were identically reproduced in both models, but differences arose as finer details were examined. However, the use of either model as input to the high-resolution IPV advection model MIMOSA appeared to reduce greatly the observed coarse grid inconsistencies, and fine coherent structures such as that observed in Figure 6b were identically reproduced when using NCEP instead of ECMWF.

[34] The next step is now to extend the current study to all years and all seasons available since the JPL lidars began operating. Better diagnostic tools will be developed in order to isolate the STE and meridional transport signatures of many processes such as for example ENSO and the QBO. Using the high resolution advection model MIMOSA together with more sophisticated trajectory diagnostics, and more sophisticated proxies on the origin and history of the air parcels sampled by lidar, we expect eventually to relate most aspects of the lidar-observed ozone variability to the associated lower and midstratospheric circulation over the central and eastern Pacific. In cases where no significant dynamical effects can be identified, we will investigate photochemical effects by using an extended transport chemistry version of MIMOSA.

[35] **Acknowledgments.** The work described in this paper was carried out at the Jet Propulsion Laboratory, California Institute of Technology, under an agreement with the National Aeronautics and Space Administration. The authors would like to thank those other members of the JPL Lidar Team, D. A. Haner, J. Howe, and T. D. Walsh, who assisted in the collection of the data used here. The ECMWF T106 data were made available for NDSC participants at the Norwegian Institute for Air Research (NILU), Norway, and the NCEP Reanalysis data were provided from the NOAA-CIRES Climate Diagnostics Center, Boulder, Colorado, USA.

References

Appenzeller, C., H. C. Davies, and W. A. Norton (1996), Fragmentation of stratospheric intrusions, *J. Geophys. Res.*, *101*, 1435–1456.

Butchard, N., and E. E. Remsberg (1986), The area of the stratospheric polar vortex as a diagnostic for tracer transport on an isentropic surface, *J. Atmos. Sci.*, *43*, 1319–1339.

Calisesi, Y., H. Wernli, and N. Kampfer (2001), Midstratospheric ozone variability over Bern related to planetary wave activity during the winters 1994–1995 to 1998–1999, *J. Geophys. Res.*, *106*, 7903–7916.

Chen, P. (1995), Isentropic cross-tropopause mass-exchange in the extratropics, *J. Geophys. Res.*, *100*, 16,661–16,673.

Chen, P., J. R. Holton, A. O'Neill, and R. Swinbank (1994), Isentropic mass-exchange between the tropics and extratropics in the stratosphere, *J. Atmos. Sci.*, *51*, 3006–3018.

Cooper, O. R., J. L. Moody, J. C. Davenport, S. J. Oltmans, B. J. Johnson, P. B. Shepson, X. Chen, and J. T. Merrill (1998), The influence of springtime weather systems on vertical ozone distributions over three North American sites, *J. Geophys. Res.*, *103*, 22,001–22,013.

Dunkerton, T. J. (1995), Evidence of meridional motion in the summer lower stratosphere adjacent to monsoon regions, *J. Geophys. Res.*, *100*, 16,675–16,688.

Fortuin, J. P. F., and H. Kelder (1998), An ozone climatology based on ozonesonde and satellite measurements, *J. Geophys. Res.*, *103*, 31,709–31,734.

Gettelman, A., M. L. Salby, and F. Sassi (2002), Distribution and influence of convection in the tropical tropopause region, *J. Geophys. Res.*, *107*(D10), 4080, doi:10.1029/2001JD001048.

Grant, W. B. (Ed.) (1989), *Ozone Measuring Instruments for the Stratosphere*, vol. 1, *Collected Works in Optics*, Opt. Soc. of Am., Washington, D. C.

Hauchecorne, A., S. Godin, M. Marchand, B. Heese, and C. Souprayen (2002), Quantification of the transport of chemical constituents from the polar vortex to midlatitudes in the lower stratosphere using the high-resolution advection model MIMOSA and effective diffusivity, *J. Geophys. Res.*, *107*(D20), 8289, doi:10.1029/2001JD000491.

Hoskins, B. J. (1991), Towards a PV-θ view of the general circulation, *Tellus*, *43*, 27–35.

Kalnay, E., et al. (1996), The NCEP/NCAR 40-year reanalysis project, *Bull. Am. Meteorol. Soc.*, *77*, 437–471.

Knudsen, B. M., J.-P. Pommereau, A. Garnier, M. Nunez-Pinharanda, L. Denis, G. Letrenne, M. Durand, and J. M. Rosen (2001), Comparison of stratospheric air parcel trajectories based on different meteorological analyses, *J. Geophys. Res.*, *106*, 3415–3424.

Koch, G., H. Wernli, J. Staehelin, and T. Peter (2002), A Lagrangian analysis of stratospheric ozone variability and long-term trends above Payerne (Switzerland) during 1970–2001, *J. Geophys. Res.*, *107*(D19), 4373, doi:10.1029/2001JD001550.

Lait, L. R. (1994), An alternative form for potential vorticity, *J. Atmos. Sci.*, *51*, 1754–1759.

Leblanc, T., and I. S. McDermid (2000), Stratospheric ozone climatology from lidar measurements at Table Mountain (34.4°N, 117.7°W) and Mauna Loa (19.5°N, 155.6°W), *J. Geophys. Res.*, *105*, 14,613–14,623.

Leblanc, T., and I. S. McDermid (2001), Quasi-biennial oscillation signatures in ozone and temperature observed by lidar at Mauna Loa, Hawaii (19.5°N, 155.6°W), *J. Geophys. Res.*, *106*, 14,869–14,874.

Mahfouf, J. F., and F. Rabier (2000), The ECMWF operational implementation of four-dimensional variational assimilation, II: Experimental results with improved physics, *Q. J. R. Meteorol. Soc.*, *126*, 1171–1190.

McDermid, I. S., S. Godin, and L. O. Lindqvist (1990), Ground-based laser DIAL system for long-term measurements of stratospheric ozone, *Appl. Opt.*, *29*, 3603–3612.

McDermid, I. S., T. D. Walsh, A. Deslis, and M. L. White (1995), Optical-systems design for a stratospheric lidar system, *Appl. Opt.*, *34*, 6201–6210.

McDermid, I. S., G. Beyerle, D. Haner, and T. Leblanc (2002), Redesign and improved performance of the tropospheric ozone lidar at the Jet Propulsion Laboratory Table Mountain facility, *Appl. Opt.*, *41*, 7550–7555.

McIntyre, M. E., and T. N. Palmer (1984), The "surf zone" in the stratosphere, *J. Atmos. Terr. Phys.*, *46*, 825–849.

Newchurch, M. J., et al. (2000), Upper-stratospheric ozone trends 1979–1998, *J. Geophys. Res.*, *105*, 14,625–14,636.

Norton, W. A. (1994), Breaking Rossby-waves in a model stratosphere diagnosed by a vortex-following coordinate system and a technique for advecting material contours, *J. Atmos. Sci.*, *51*, 654–673.

Orsolini, Y., and W. B. Grant (2000), Seasonal formation of nitrous oxide laminae in the mid and low latitude stratosphere, *Geophys. Res. Lett.*, *27*, 1119–1122.

Postel, G. A., and M. H. Hitchman (1999), A climatology of Rossby wave breaking along the subtropical tropopause, *J. Atmos. Sci.*, *56*, 359–373.

Rabier, E., H. Jarvinen, E. Klinker, J. F. Mahfouf, and A. Simmons (2000), The ECMWF operational implementation of four-dimensional variational assimilation, I: Experimental results with simplified physics, *Q. J. R. Meteorol. Soc.*, *126*, 1143–1170.

Reid, S. J., and G. Vaughn (1991), Lamination in ozone profiles in the lower stratosphere, *Q. J. R. Meteorol. Soc.*, *117*, 825–844.

Reinsel, G. C., et al. (1999), Update of Umkehr ozone profiles data trend analysis through 1997, *J. Geophys. Res.*, *104*, 23,881–23,898.

Remsberg, E. E., P. P. Bhatt, and L. E. Deaver (2001), Ozone changes in the lower stratosphere from the Halogen Occultation Experiment for 1991–1999, *J. Geophys. Res.*, *106*, 1639–1653.

Semane, N., H. Teitelbaum, and C. Basdevant (2002), A very deep ozone minihole in the Northern Hemisphere stratosphere at mid-latitude during the winter 2000, *Tellus, Ser. A*, *54*, 382–389.

Shuckburg, E., W. Norton, A. Iwi, and P. Haynes (2001), Influence of the quasi-biennial oscillation on isentropic transport and mixing in the tropics and subtropics, *J. Geophys. Res.*, *106*, 14,327–14,337.

Simmons, A. J., and A. Hollingsworth (2002), Some aspects of the improvement in skill of numerical weather prediction, *Q. J. R. Meteorol. Soc.*, *128*, 647–677.

Stohl, A. (1998), Computation, accuracy and applications of trajectories—A review and bibliography, *Atmos. Environ.*, *32*, 947–966.

Stohl, A., and P. Seibert (1998), Accuracy of trajectories as determined from the conservation of meteorological tracers, *Q. J. R. Meteorol. Soc.*, *124*, 1465–1484.

Thorncroft, C. D., B. J. Hoskins, and M. F. McIntyre (1993), Two paradigms of baroclinic-wave life-cycle behavior, *Q. J. R. Meteorol. Soc.*, *119*, 17–55.

Trepte, C. R., R. E. Veiga, and M. P. McCormick (1993), The poleward dispersal of Mt. Pinatubo volcanic aerosol, *J. Geophys. Res.*, *98*, 18,563–18,573.

Waugh, D. W. (1996), Seasonal variation of isentropic transport out of the tropical stratosphere, *J. Geophys. Res.*, *101*, 4007–4023.

Waugh, D. W., and B. M. Funatsu (2003), Intrusions into the tropical upper troposphere: Three dimensional structure and accompanying ozone and OLR distributions, *J. Atmos. Sci.*, *60*, 637–653.

Waugh, D. W., and L. M. Polvani (2000), Climatology of intrusions into the tropical upper troposphere, *Geophys. Res. Lett.*, *27*, 3857–3860.

World Meteorological Organization (WMO) (1957), Definition of the tropopause, *WMO Bull.*, *6*, 136.

A. Hauchecorne, Service d'Aeronomie du CNRS, BP3, F-91371 Verrieres-le-Buisson cedex, France.

T. Leblanc and I. S. McDermid, Table Mountain Facility, Jet Propulsion Laboratory, California Institute of Technology, Wrightwood, CA 92397-0367, USA. (leblanc@tmf.jpl.nasa.gov)